Fe(II)-loaded goat manure biochar efficiently activated peroxymonosulfate for tetracycline degradation in groundwater

Lianjie Fan[1,2,3], Qinglin Xie[1]*, Yanhong Li[1], Shengzhang Zou[2,3], Haiping Lu[2,3], Su Ling Li[1,2] and Xiaoxiao Li[4]*

[1]College of Environmental Science and Engineering, Guilin University of Technology, Guilin, China, [2]Guangxi Karst Resources and Environment Research Center of Engineering Technology, Institute of Karst Geology, Chinese Academy of Geological Sciences, Guilin, China, [3]International Research Centre on Karst under the Auspices of UNESCO, National Center for International Research on Karst Dynamic System and Global Change, Guilin, China, [4]College of Environment, Hohai University, Nanjing, China

Poultry manure is one of the important sources of antibiotic pollution in agricultural soil and groundwater. Recently, the excessive discharge of goat manure has resulted in groundwater environmental challenges and negative impacts. It is of practical significance that such wastes can be converted into functional materials to promote the resource utilization of waste and reduce the risk of antibiotic contamination. In this study, Fe (II)-loaded goat manure biochar (Fe-GMC) was prepared by pyrolyzing goat manure and iron salts and used to activate peroxymonosulfate (PMS) for tetracycline (TC) degradation in groundwater. The as-prepared Fe-GMC exhibited good catalytic performance for PMS activation due to its porous surface and rich oxygen-containing groups. Under the conditions of catalyst dosage of 0.2 g/L, PMS dosage of 1.0 mM, and pH of 3.0, TC was removed 81.3% within 60 min. In addition, the TC degradation efficiency was inhibited to different extents by inorganic anions ($HCO_3^- > Cl^- > NO_3^-$) in water. Furthermore, the quenching experiments, electron paramagnetic resonance (EPR) experiments, and X-ray photoelectron spectroscopy (XPS) spectra analysis indicated that the generation of hydroxyl radicals ($^\bullet OH$) was responsible for TC degradation. Particularly, Fe-GMC produces a strong oxidizing agent. This study provides an efficient and environmentally friendly tetracycline degradation catalyst, which offers a new theoretical basis for water environmental remediation.

KEYWORDS

goat manure, tetracycline degradation, waste utilization, Fe(III), peroxymonosulfate
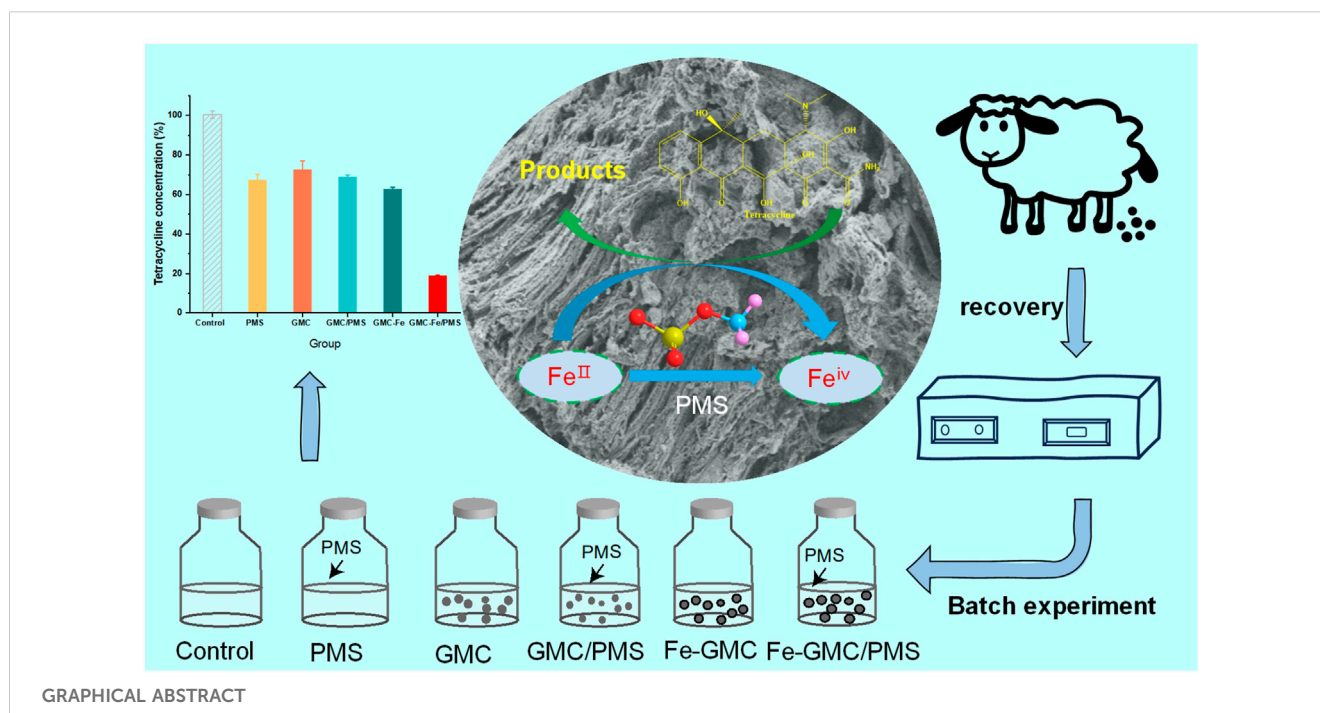
GRAPHICAL ABSTRACT

1 Introduction

Antibiotics are chemical agents used to treat microbial infectious diseases and are widely used in human and animal healthcare and aquaculture. Due to their long stability and extensive distribution characteristics, antibiotics have become a worldwide pollutant (Jiang L. B. et al., 2018; Zhang et al., 2019). Tetracyclines (TCs) are widely used for treating and preventing animal diseases, promoting animal growth, and improving animal husbandry productivity. They represent the largest class of veterinary antibiotics used in China's livestock and poultry industry, accounting for approximately 37% of the total antibiotic use. However, TC antibiotics cannot be completely absorbed by the animal body and are excreted in the form of maternal or metabolites with livestock and poultry manure. Antibiotics discharged from livestock feedlots through wastewater could disseminate into surrounding groundwater environments (Xiao et al., 2018, Watanabe et al., 2010). Thermophilic composting has proven to be a cost-effective technology for recovering animal manure resources and mitigating TC-related hazards, but there are problems with higher costs and incomplete removal (Wanying et al., 2023). Thus, TC is detected in large quantities in environmental media such as water, sediments, and soil. Therefore, there is an urgent need to develop an economical and environmentally friendly approach to control TC pollution (Zhijie et al., 2018; Wang and Wang, 2018).

To date, adsorption (Rahmat and Ahmadi, 2019), biological treatment (Xiaodong et al., 2021), advanced oxidation processes (AOPs), and other techniques have been employed to treat TC (Dong et al., 2017; Hussain et al., 2017). AOPs have attracted widespread attention because of their high efficiency in the degradation of TC (Yangju et al., 2021). Therein, PMS-based

AOPs are regarded as optimized means to remove refractory contaminants, benefiting from the strong oxidation ability, excellent stability, and convenient transportation (Chang-Mao et al., 2016; Luo et al., 2020). Moreover, PMS could be activated to produce radicals (sulfate radical $SO_4^{\bullet-}$), hydroxyl radical ($^{\bullet}OH$), superoxide radical ($O_2^{\bullet-}$), and singlet oxygen ($^1O_2$) (Zou et al., 2019; Wang et al., 2017). Therefore, compared with the Fenton reaction, the PMS activation process has a stronger mineralization capacity. Fe^{2+} is the best reagent for PMS activation because Fe^{2+} is inexpensive, environmentally friendly, and non-biotoxic (Zhu et al., 2022). In addition, a non-radical pathway occurs during the reaction, and the intermediate reactant, high-valent iron (Fe(IV)), has attracted widespread attention due to its strong oxidation potential (Xingyu et al., 2022).

PMS could be activated by UV, heat, ultrasound, and transition metals. Although UV is an efficient method to activate PMS, its low economic benefits limit its widespread application (Wang et al., 2018). Thus, ferrous iron (Fe (II)) was commonly chosen as the activator for $SO_4^{\bullet-}$ generation from PMS due to its advantages of environmental friendliness, cost-effectiveness, and high activity (Uthirakrishnan et al., 2020). At present, carbon matrices such as graphene and carbon nanotubes are widely used (Xiao et al., 2018). However, their development costs are more expensive. Consequently, low-cost carbon materials should be developed. Biochar provides new active points for PMS due to its huge specific surface area, abundant oxygen-containing functional groups, and hybrid carbon structure, which can be considered sustainable and promising catalyst support (Bolan et al., 2022).

With the development of animal husbandry, the excessive discharge of animal manure has placed a severe burden on the environment (Zhu et al., 2013). Research has explored biochar-loaded Fe-based activation of PMS to generate free radicals for

pollutant removal from water. Studies such as those by Wu et al. (2023) and Fang et al. (2024) have shown that this approach can generate $SO_4^{\bullet-}$ and $\cdot\bullet OH$ free radicals, which effectively remove pollutants from water. However, limited research has focused on "Waste for Waste" methods to produce biochar. The "Waste for Waste" paradigm represents an ecologically sound and sustainable developmental ideology, accentuating the conversion of waste into valuable resources. Goat manure is a valuable option as a carbon matrix for the removal of tetracycline by activating PMS. On one hand, this approach can reduce antibiotic contamination of goat manure itself. On the other hand, we can make full use of the small number of inherent heteroatoms in goat manure to avoid additional doping, thereby contributing to antibiotic removal from the environment (Wang et al., 2021; Miguel et al., 2022). Therefore, the resource utilization of goat manure not only reduces environmental pollution but also offers practical advantages. Goat manure is widely available, has low price, and can be produced on a large scale. In this study, a novel Fe-GMC material was synthesized using goat manure and $FeSO_4.7H_2O$ as feedstocks and was used to activate PMS for TC degradation. The key factors affecting the degradation of TC in the Fe-GMC/PMS system, such as initial pH, PMS dosage, Fe-GMC dosage, inorganic ions, and reaction temperature, were also investigated. Finally, the oxidation pathways and mechanism of the Fe-GMC/PMS system were elucidated through scavenging tests and electron paramagnetic resonance (EPR).

2 Experimental

2.1 Materials

The raw goat manure was obtained from the local farm in Yunnan. The collected goat manure was rinsed with deionized water and dried at 60°C for subsequent use. Ferrous sulfate ($FeSO_4 \cdot 7H_2O$) and tetracycline (TC) were purchased from Aladdin Chemistry Co. Ltd., China. Other compounds including $2KHSO_5 \cdot K_2SO_4 \cdot K_2SO_4$ (PMS), sodium chloride (NaCl), sodium bicarbonate ($NaHCO_3$), sodium nitrate ($NaNO_3$), ethanol (Et-OH), and tert-butanol (TBA) were supplied by Sinopharm Chemical Reagent Co. Ltd. (Shanghai, China). All reagents were of analytical grade and used directly without further purification. The aqueous solution involved in the experiments was prepared with deionized water produced in the laboratory (Jianghui et al., 2022).

2.2 Catalyst synthesis

Fe-GMC was prepared as follows: first, 20 g of goat manure was immersed in the Fe^{2+} solution (0.05 M) under continuous stirring overnight, followed by washing twice with deionized water and drying at 60°C (Luo et al., 2020). Afterward, the obtained samples were placed in the quartz boat and carbonized in a tube furnace at 800°C (at a rate of 5°C/min) for 2 h under the continuous nitrogen atmosphere. The furnace was allowed to cool, and the sample was removed and placed inside a sample bag. The prepared sample was referred to as Fe-GMC. Raw goat manure (GMC) was prepared without iron.

2.3 Catalyst characterization

X-ray diffraction (XRD, Bruker D8) was conducted to confirm the crystal structure of Fe-GMC and GMC. The morphologies and structural features of Fe-GMC and GMC were determined via scanning electron microscopy (SEM; Zeiss Sigma HD, Germany) with an X-ray energy dispersive spectrometer (EDS). High-resolution transmission electron microscopy (TEM, FEI Talos F200x, United States) tests were utilized to observe the micro shape on catalyst surface. The surface elements of the Fe-GMC were recorded by X-ray photoelectron spectroscopy (XPS; ESCALAB250Xi, Thermo Fisher). Fourier transform infrared spectroscopy (FT-IR) was utilized to monitor the functional groups of the composites. Electron paramagnetic resonance (EPR, JEOL JES-FA200) examined the main active species. Brunauer–Emmett–Teller (BET) surface area was employed to obtain the specific surface area.

2.4 Catalytic activity experiment

Fe-GMC was ground into powder and used in the batch catalytic experiments. In brief, the reactions were carried out in the 125 mL serum bottle TC (10 mg/L, 50 mL) and PMS (1.0 mM), which were initiated by adding 0.1 g of catalyst into the TC solution, which was shaken by a thermostatic reciprocating shaker at 150 rpm and 30°C. All serum bottles were covered with tin foil. At different elapsed times, a 2 mL sample was collected from each flask using a 10 mL syringe. After that, the remaining concentration of TC was measured using a UV–Vis spectrophotometer at 357 nm. The reaction kinetics of TC was simulated using the pseudo-first kinetic model. Details related to the model are provided as Text S1 in Supporting Information.

The key factors affecting the degradation of TC in the Fe-GMC/PMS system, such as initial pH, PMS dosage, Fe-GMC dosage, inorganic ions, and reaction temperature, were determined and detailed in SI (Supporting Information, see Text S2). In quenching experiments, Et-OH ($SO_4^{\bullet-}$ and $^\bullet OH$), TBA ($SO_4^{\bullet-}$), and L-histidine ($^1O_2$) were selected as quenchers to scavenge corresponding active species. Afterward, the process was monitored using the UV–Vis spectrophotometer.

3 Results and discussion

3.1 Material characterization

Figure 1A shows that the surface morphologies and structure of materials were confirmed via SEM. The SEM results determined that goat manure without supported iron exhibited a smooth surface with an irregular multilayer lamellar structure and some stripes (Figure 1A). In contrast, for Fe-GMC, some pores and ridges can be seen in Figure 1B, which increases the active sites and is more conducive to the adsorption of TC (Mingfei et al., 2021). The detailed elemental distribution and content of Raw goat manure and Fe-GMC were determined by EDS (Figures 1C, D). The element Fe was detected, which indicated the successful introduction of Fe species. Uniformly distributed Fe nanoparticles can be seen in

FIGURE 1
SEM images of **(A)** raw goat manure and **(B)** Fe-GMC and **(C)** raw goat manure and **(D)** Fe-GMC EDS. **(E)** TEM and HRTEM **(F)** images of Fe-GMC.
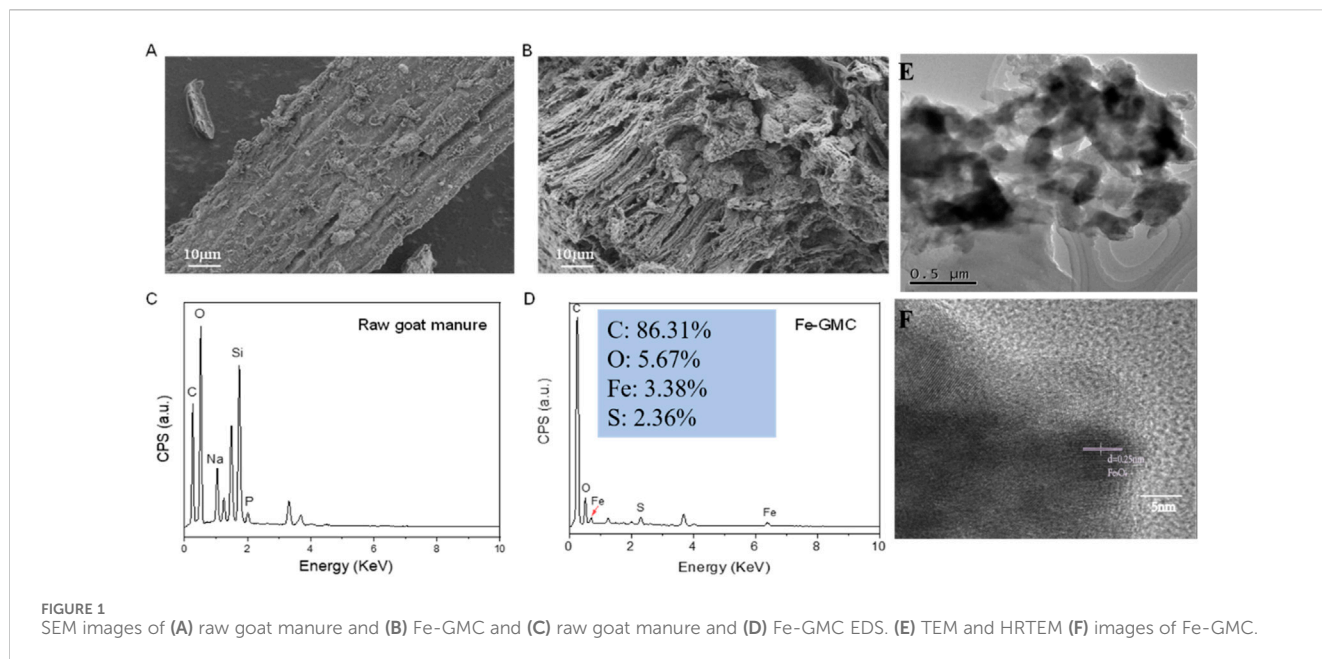
Figure 1E, demonstrating that Fe particles are encapsulated within the GMC. As indicated by the high-magnification TEM image (Figure 1F), a thin layered structure of carbon nanoflakes could be observed, with a lattice spacing of 0.25 nm attributed to Fe_3O_4, similar to previous studies (Wang et al., 2020). In addition, the layered nanoflake structures are highly porous and become gradually thinner toward the edges of the material. Moreover, these uniformly distributed Fe_3O_4 particles onto the biochar carrier corroborated the results of SEM images of Figure 1B, and this study demonstrates the successful synthesis of Fe-GMC composites.
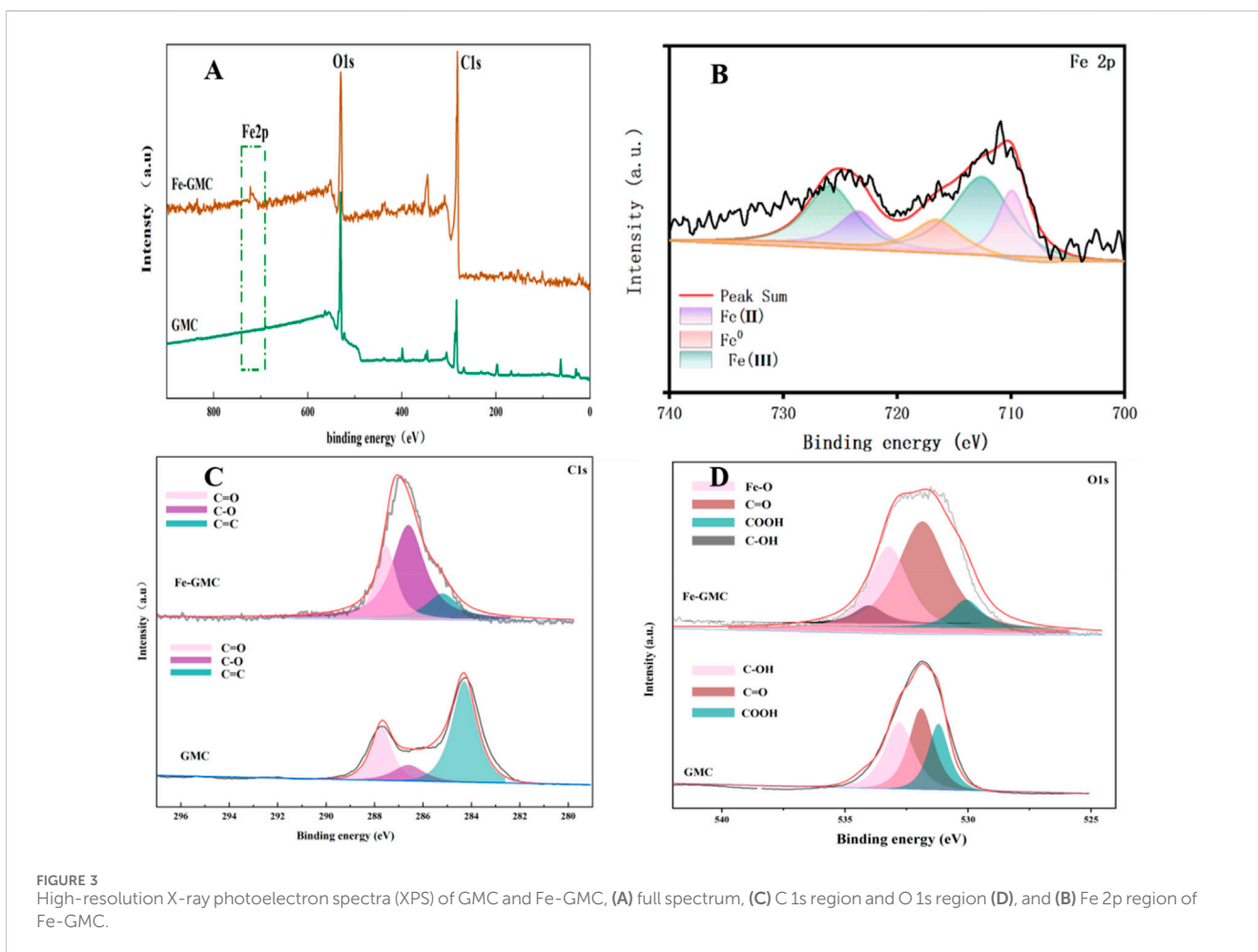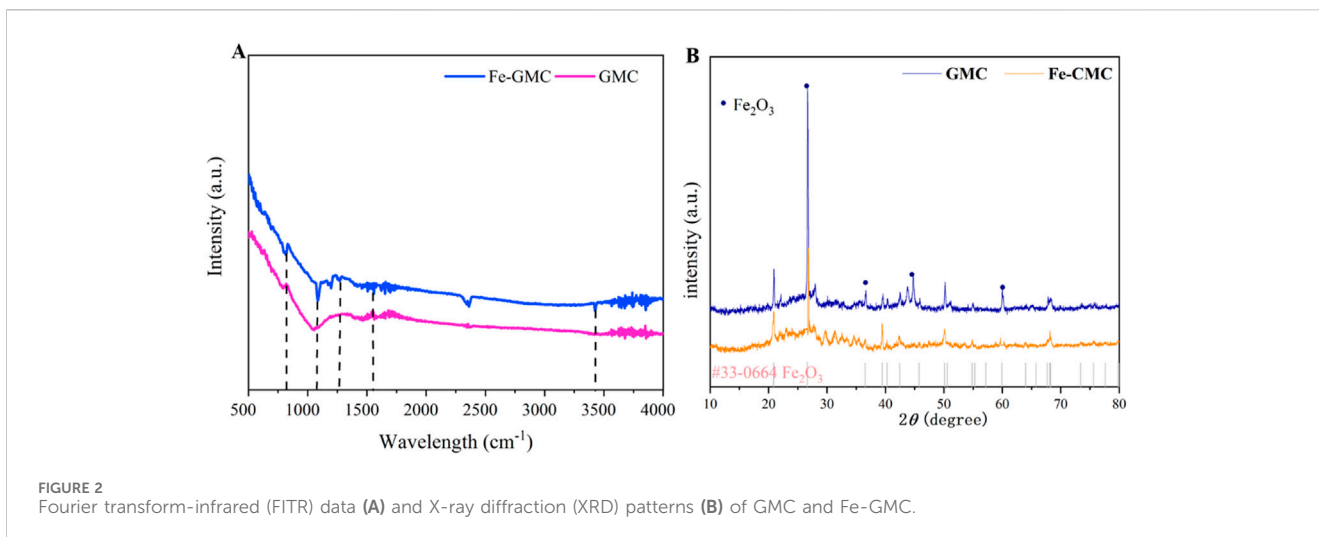
The surface functional groups were investigated by FT-IR. As observed in Figure 2A, the stretching vibration of C=O and C=C bonds transformed from aromatic rings results in a signal at 1,623 cm^{-1} (Pu et al., 2021). The C–C stretching vibration was observed at 1,172 cm^{-1}, and the band at 1,084 cm^{-1} corresponded to the C–O stretching vibration (Tianyi et al., 2020). The pyrolysis of organic to obtain the biochar played an important role in increasing oxygen-containing surface functional groups, and this might enhance the biochar activation effect (Dong et al., 2017). In addition, there was an obvious vibration at approximately 570 cm^{-1} for Fe-GMC, which indicated the existence of an Fe-O characteristic peak in Fe-GMC, which also suggested that Fe^{2+} was successfully synthesized on the GMC (Jayaselvan L et al., 2020). In summary, the Fe-GMC had abundant oxygen-containing functional groups and oxides of Fe (II)/Fe (III). Furthermore, the crystal phase composition of the composite was determined by XRD (Shuzhao et al., 2020). Figure 2B shows a diffraction peak of Fe-GMC with a 2θ value of 43.74, 44.76, and 45.1, which corresponds to Fe_3C (Tang et al., 2021; Chen et al., 2022). In addition, the dominant Fe_3O_4 diffraction peaks were detected at 2θ values of approximately 35.49 plane (Ikramullah and Zulkarnain, 2019). This result indicated that Fe-GMC may be loaded Fe_3O_4. The diffraction peaks at 26° and 60° are assigned to Fe_2SiO_4 and magnetite, respectively, and the inorganic mineral composition Fe_2SiO_4 was

detected in Fe-GMC. This might be due to the redox reaction between Fe and Si components during high-temperature pyrolysis, and there is a significant increase in the XRD peak after the composite, indicating the successful composite of Fe_3O_4 (Song et al., 2022).

Similarly, we analyzed the specific surface area of the loaded material, as shown in Supplementary Figure S1, and the Fe-GMC composites exhibit type IV adsorption curves and H3 type hysteresis loops, indicative of mesoporous attributes. In addition, the material has a good specific surface area and pore structure, with experimental results indicating a specific surface area of 416.248 m^2/g. This finding summarizes the physical properties of the material, making it suitable for adsorption, catalysis, and composite superiority of the material.

To further analyze the material's surface chemical compositions, XPS analysis was conducted. As shown in Figure 3, the XPS full-spectrum and the spectra of Fe 2p, C 1 s and O 1 s in the Fe-GMC sample were obtained. The XPS spectra (Figure 3A) confirmed the presence of C (284.8 eV) and O (531.8 eV). Compared with the full spectrum of GMC, Fe-GMC exhibited a distinct characteristic peak at 724.6 ev, which is the characteristic peak of Fe, consistent with the results of EDS characterization (Figure 1C). In Figure 3B, Fe 2p spectrum shows peaks at 710.45 eV and 724.1 eV (due to Fe $2p_{3/2}$) and 711.85 eV and 726.3 eV (corresponded to Fe $2p_{1/2}$), while the peaks at 718.5 eV and 733.0 eV were the satellite peaks of Fe $2p_{3/2}$ to Fe $2p_{1/2}$, respectively (Mohammadi and Saied Saeed Hosseiny, 2020). The peak area ratio of Fe^{2+} to Fe^{3+} obtained from the XPS analysis was close to 1:2. This result was also consistent with the abovementioned XRD analysis results, which verify the presence of Fe_3O_4 particles on the surface of Fe-GMC.

To facilitate the differentiation of the materials prior to and following the composite formation for further study, C 1 s and O 1 s spectra of biochar and the composites are separated into several fine peaks. From Figures 3C,D, it can be concluded that with the addition of Fe_3O_4, the positions of the peaks of the oxygen-containing

FIGURE 2
Fourier transform-infrared (FITR) data **(A)** and X-ray diffraction (XRD) patterns **(B)** of GMC and Fe-GMC.

FIGURE 3
High-resolution X-ray photoelectron spectra (XPS) of GMC and Fe-GMC, **(A)** full spectrum, **(C)** C 1s region and O 1s region **(D)**, and **(B)** Fe 2p region of Fe-GMC.

functional groups in the composites are generally to the left, and the binding energy increases. It can also be observed from Figure 3D that the relative area of C-OH in Fe-GMC decreases, while the relative area of Fe-O increases, indicating that the oxygen-containing functional groups on the GMC play important roles in the composite of Fe_3O_4. These findings are similar to those of previous studies (Song et al., 2019). At the same time, the electron-rich groups C=C and C=O can favor the activation of PMS to produce free radicals, and these free radicals may facilitate TC removal (Chen et al., 2020; Luo et al., 2020; Zou et al., 2019). These conclusions can be a good proof of the success of the material composite.
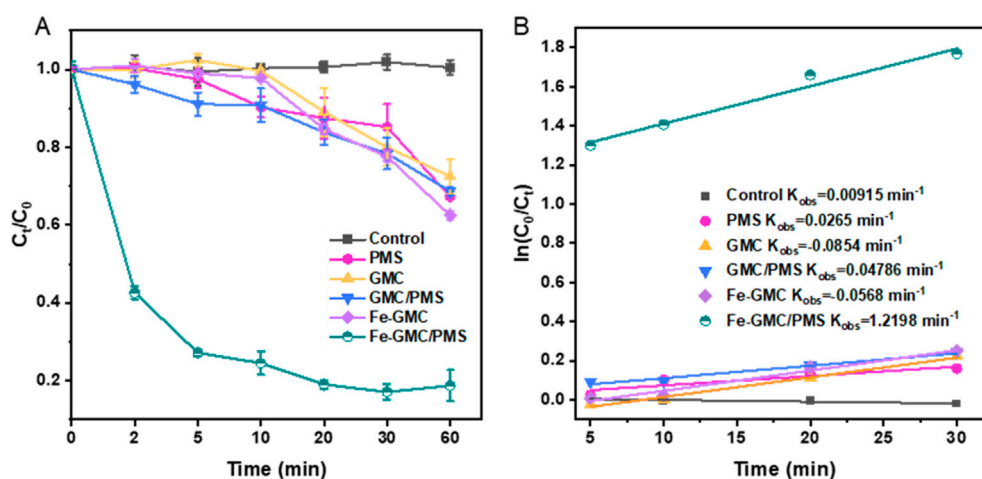
FIGURE 4
TC removal in different systems **(A)** and the pseudo-first order kinetic fitting curves **(B)** (experiment conditions: 0.20 g/L catalyst, 1 mM PMS, initial pH = 3.01, and 30°C).

3.2 Catalytic activity of Fe-GMC

3.2.1 Performance of Fe-GMC catalytic degradation of TC

TC was selected as the target pollutant to measure the catalytic activity of Fe-GMC. The results of the degradation of the TC solution are shown in Figure 4A and Supplementary Table S1. It is evident that the addition of Fe-GMC resulted in a significant increase in TC removal. In the reaction system containing GMC, the removal rate of TC by PMS was determined to be 31.3%. In the GMC system with Fe^{2+}, the maximum removal rate of TC due to pure adsorption is only 37.5% in the absence of PMS. When PMS was added, the degradation rate of TC reached 81.3% in 60 min. In addition, the reaction kinetics of the Fe-GMC systems was analyzed according to a pseudo-first order reaction model (Figure 4B; Supplementary Table S2). The apparent rate constants were calculated to be 0.0092 min^{-1} for control, 0.0479 min^{-1} for the GMC/PMS system, and 1.2198 min^{-1} for the Fe-GMC/PMS system. It was clear that Fe-GMC/PMS showed the highest apparent degradation rate constant, about 25.95 times higher than GMC-PMS. It has been previously reported that the synergic effect between Fe and biochar resulted in high catalytic performance via producing radicals and non-free radicals in the presence of PMS (Zang et al., 2020).

3.2.2 Influence of different parameters on TC degradation

Different experimental parameters, including catalyst and PMS concentration, reaction temperature, initial solution pH, and inorganic anions, are analyzed to explore the catalytic properties of the Fe-GMC/PMS system (Figure 5, Supplementary Table S3, Supplementary Figure S2). The effect of catalyst dose on TC degradation was displayed in Figure 5A and Supplementary Table S3. The removal efficiency of TC increased from 78.1% to 81.3% when the catalyst dose increased from 0.05 to 0.20 g/L in 60 min, which could be because increasing the catalyst dosage could offer more active sites to activate PMS and lead to the generation of

more radicals (Alireza et al., 2015). However, as the dosage of the catalyst continued to increase to 0.25 g/L, TC degradation decreased from 81.3% to 79.5%. Further increases in the biochar dose may overproduce oxidizing free radicals, promoting interactions between free radicals and leading to reduced pollutant decomposition (Nguyen et al., 2019). The abovementioned difference in TC removal from 78.1% to 81.3% was too slight because of the excessive generation of reactive oxygen radicals by Fe-GMC/PMS. For this reason, we increased the initial concentration of TC and the reaction time to identify the optimal concentration of catalyst addition, which can be observed in Supplementary Figure S3. When the TC concentration was 15 mg/L, the 0.2 mg/L catalyst could remove 66% of the TC in 120 min, which was much more than the other catalyst additions, and for this reason, the 0.2 mg/L catalyst was chosen for the following experiments.

The impact of the PMS concentration on TC removal is illustrated in Figure 5B. The removal rate of TC increases correspondingly as the initial PMS concentration increases. At an initial PMS concentration of 0.5 mM, the removal rate of TC is low, and only 48.8% of TC is removed over 60 min. When PMS concentration increased to 1 mM, the removal rate increased to 81.3%. However, when 2 mM of PMS was added, the degradation efficiency was not improved. The results may be attributed to the significant self-quenching effect (Haitao et al., 2020). The degradation efficiencies were increased from 71.2% to 81.3% with the increase in reaction temperatures from 10°C to 30°C (Figure 5C), which indicated that a higher reaction temperature accelerates the decomposition of PMS, generating more free radicals $^{\bullet}OH$ and $SO_4^{\bullet-}$ for TC degradation. However, excessively high temperatures (60°C) can destroy free radical activity (Ruan et al., 2019).

The initial pH can affect the release of ferrous ions and the activity of oxidants in Fe-GMC (Ma et al., 2021). Therefore, it is necessary to explore the effect of different initial pH values on TC removal. Figure 5D illustrates that the degradation efficiencies for TC were 81.3%, 66.5%, 47.5%, and 37.1% within the Fe-GMC/PMS system when the initial pH values were 3.0, 5.0, 7.0, and 11.0, respectively. Since the surface charge of biochar is positive when the
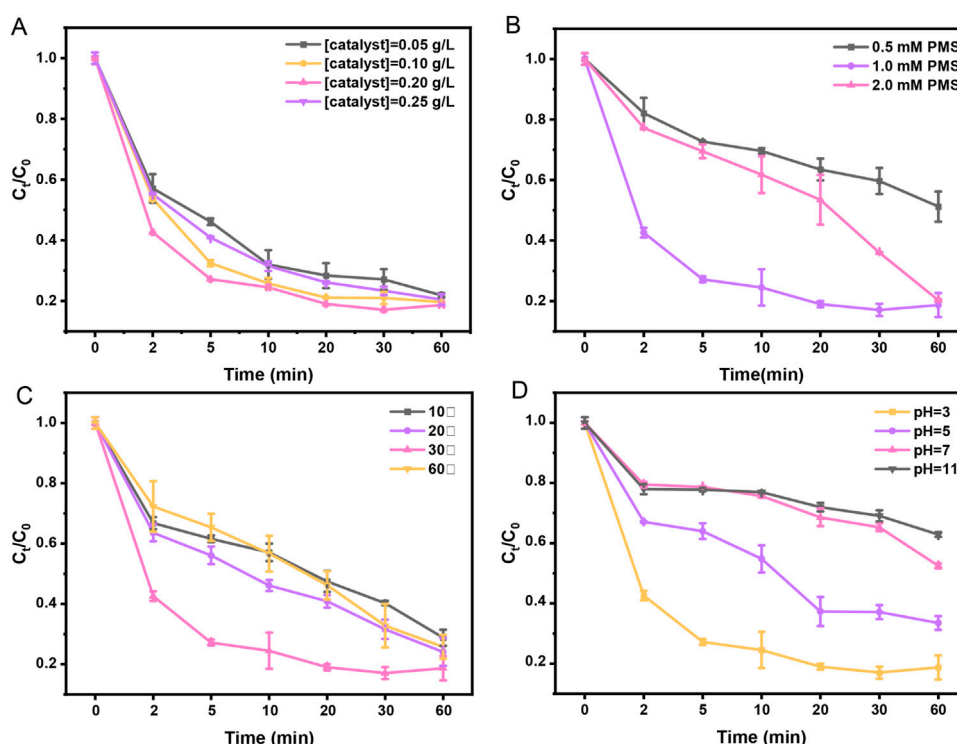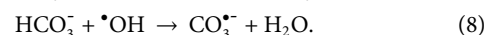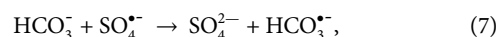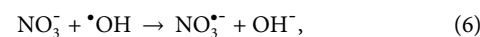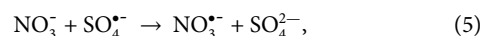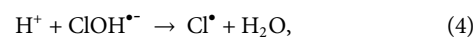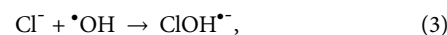
FIGURE 5
Effect of experimental conditions on TC removal in the Fe-GMC/PMS system. **(A)** Catalyst dosage (0.05 g/L−0.25 g/L), **(B)** PMS dosage (0.5−2.0 mM),
(C) reaction temperature (10°C−60°C), and **(D)** initial pH (3−11).

initial pH value is 3.0, it is conducive to the approach of PMS to the surface of biochar (Da et al., 2019). However, as the initial pH gradually increases (pH 5–11), the negative charge on the surface of biochar increases, hindering its reaction with PMS (Ahmadi and Farshid, 2019).

Usually, many anions are ubiquitous in the real water environment, and their presence can affect catalytic activity. Therefore, the effects of Cl^-, NO_3^-, and HCO_3^- on TC degradation were studied. As demonstrated in Supplementary Table S3 and Supplementary Figure S2, it was found that three typical inorganic anions had an inhibitory effect on TC removal, and the removal efficiencies of TC were 52.2%, 60.3%, and 44.9% within 60 min, respectively. At the same time, we explored the effect of different concentrations of inorganic anions on the removal of TC from the system (Supplementary Figure S4), and the results demonstrated that the inhibition of TC removal remained relatively consistent when the concentration of inorganic anions was increased from the low-concentration condition, which was attributed to the fact that •OH was replaced by the reactive species with much smaller redox potentials. NO_3^- and Cl-have a slight inhibition on TC removal, which is due to the fact that these anions could scavenge free radicals and form weak radical species [Equations (1–5)] (Masoumeh et al., 2018). However, HCO_3^- had a serious inhibitory effect on TC degradation, which could scavenge •OH and $SO_4^{•-}$ with high rates [Equations (1–8)]. According to the abovementioned results, different anions have a certain influence on the free radical oxidation process. Hence, studying the influence of

anions on TC degradation is conducive to providing a theoretical basis for practical applications.

Dissolved organic matter, particularly humic acid (HA), was widely present in natural water bodies. The effect of different concentrations of HA on the removal of TC by Fe-GMC/PMS was explored (Supplementary Figure S4D). The ability of carbon materials to catalyze PMS and free radical generation is reduced because HA occupies the active sites on the carbon materials. Furthermore, HA formed stable complexes with Fe^{2+} ions. This complexation hampered the release of Fe^{2+}, thereby impeding electron transfer and radical generation pathways (Li et al., 2024).

$$Cl^- + SO_4^{•-} \rightarrow Cl^• + SO_4^{2-}, \tag{1}$$

$$Cl^• + Cl^- \rightarrow Cl_2^{•-}, \tag{2}$$

$$Cl^- + {}^•OH \rightarrow ClOH^{•-}, \tag{3}$$

$$H^+ + ClOH^{•-} \rightarrow Cl^• + H_2O, \tag{4}$$

$$NO_3^- + SO_4^{•-} \rightarrow NO_3^{•-} + SO_4^{2-}, \tag{5}$$

$$NO_3^- + {}^•OH \rightarrow NO_3^{•-} + OH^-, \tag{6}$$

$$HCO_3^- + SO_4^{•-} \rightarrow SO_4^{2-} + HCO_3^{•-}, \tag{7}$$

$$HCO_3^- + {}^•OH \rightarrow CO_3^{•-} + H_2O. \tag{8}$$

The reusability of a catalyst is a crucial element in the overall assessment of its efficacy in practical applications, particularly when the financial implications are taken into account. The objective of this study was to conduct five recycling experiments under optimal conditions to further explore the stability of Fe-GMC. Figure 6A demonstrates that following five cycles of recycling, the Fe-GMC
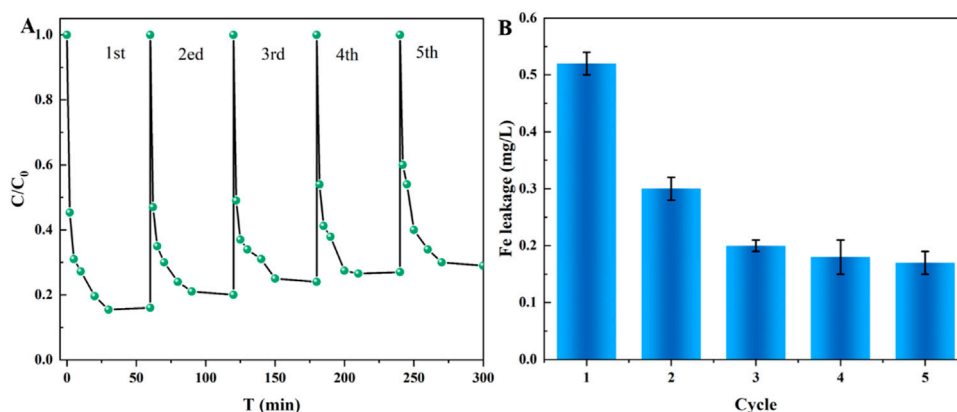
FIGURE 6
(A) Reusability of Fe-GMC/PMS for TC removal over five cycles and **(B)** Fe ion leakage during each cycle.

TABLE 1 Comparison of Fe-GMC with other reported catalysts for contaminant degradation in different systems.

Catalyst	Pollutant	Property	Recyclability	Main ROS or site	Reference
Magnetic biochar (MBC)	Tetracycline	80% in 120 min	Four times recycled with 55% removal	$O_2^{\bullet-}$, $\bullet OH$, $SO_4^{\bullet-}$, and $^1O_2$	Luo et al. (2021)
D-FeTiO3/C	Tetracycline	90% in 120 min	Five times recycled with 70% removal	$O_2^{\bullet-}$, $\bullet OH$, $SO_4^{\bullet-}$, and $^1O_2$	Luo et al. (2023)
Goethite/biochar	Tetracycline	66% in 60 min	Three times recycled with 55% removal	$\bullet OH$, $SO_4^{\bullet-}$, and $^1O_2$	Guo et al. (2021)
Fe-GMC	Tetracycline	81% in 60 min	Five times recycled with 55% removal	$\bullet OH$	This work

composites exhibit a residual TC removal rate of approximately 75%, indicative of exceptional material stability and recycling performance. This provides a robust economic foundation for practical applications. Figure 6B illustrates the leaching rate of Fe ions across each cycle of the experiment. It can be observed that the leaching of each cycle is less than 0.6 mg/L, a figure that is considerably lower than the European standard of 2 mg/L. Moreover, the Fe-GMC/PMS catalyst was evaluated in comparison to other catalysts, and the system demonstrated remarkable stability and catalytic efficacy (Table 1). Moreover, the mineralization rate of TC by the system was examined. As illustrated in Supplementary Figure S5, the total organic carbon (TOC) of TC remained at 1.6 mg/L after 60 min, and the mineralization rate was 73.37%, indicating an effective TC removal rate.

To gain a more detailed understanding of the reusability properties of Fe-GMC, the TEM, XPS, and XRD patterns of the Fe-GMC material were compared before and after five cycles of the reaction. TEM (Supplementary Figures S6A, B) demonstrated that the composite material retained its structural integrity after five cycles of the reaction, with a substantial number of Fe nanoparticles still encapsulated within the material. XPS (Supplementary Figures S6C, D) revealed that a portion of Fe(II) remained within the material, a finding that was corroborated by XRD (Supplementary Figure S6E). The intensity of the Fe₃C and Fe₃O₄ peaks exhibited a slight reduction following the reaction compared to unreacted Fe-GMC. This observation can be attributed to the decline in the removal rate observed after five cycles. The findings of this study illustrate the favorable stability and reusability of the material.

3.3 Catalytic degradation mechanism

To identify the mechanism of TC degradation in the Fe-GMC/PMS system, the contribution of related radicals in the system was differentiated by different quenching experiments (Guangfei et al., 2020). According to previously reported studies, alcohols with α-H (such as Et-OH) are capable of reacting with both $^\bullet OH$ and $SO_4^{\bullet-}$. TBA was employed as a radical $^\bullet OH$ scavenger. L-histidine (L-His) was used to prove the existence of $^1O_2$, and p-benzoquinone (p-BQ) was used to prove the existence of $O_2^{\bullet-}$ radicals (Luo et al., 2020). As shown in Figure 7A, the reaction was significantly inhibited when Et-OH was added to the system. Only 27.7% of TC was removed within 60 min. Furthermore, TBA also showed an intense inhibition on TC degradation, and the removal rate was 37.9%. In addition, to consider the possible presence of $^1O_2$ and $O_2^{\bullet-}$ in the system, p-BQ and L-His were separately added into the solution, both of which showed slight inhibitions on the oxidation process. Furthermore, p-BQ and L-His were added to the solution to verify the presence of $^1O_2$ and $O_2^{\bullet-}$, respectively, which did not show any inhibition of TC degradation. These results indicated that $SO_4^{\bullet-}$ and $^\bullet OH$ were involved in the activation of PMS, and $^\bullet OH$ was the main contributor. In general, due to the acidic environment, $^\bullet OH$ should not theoretically dominate in the Fe-GMC/PMS systems.

Fe(IV) has been reported as an emerging and powerful oxidant with higher selectivity compared to $SO_4^{\bullet-}$ and $^\bullet OH$(Wang et al., 2022). To further verify the generated radicals in the degradation reaction, an ESR test was coupled
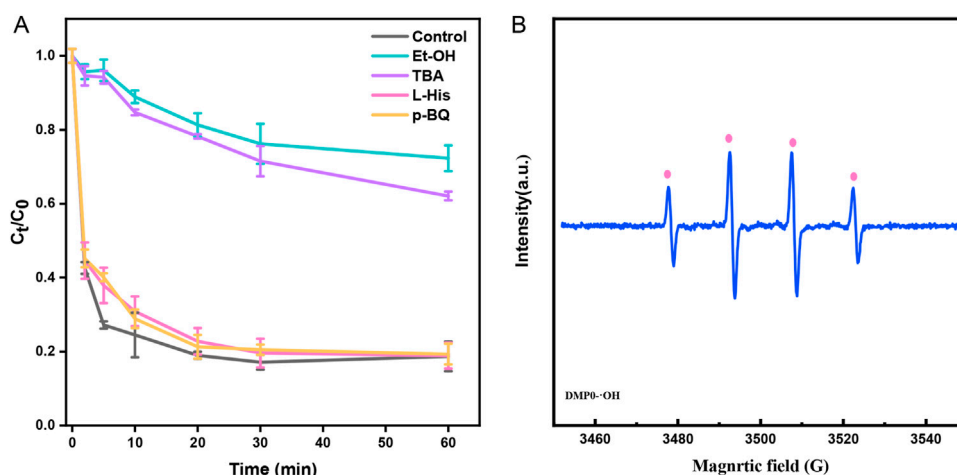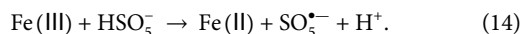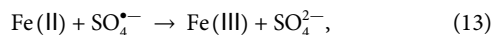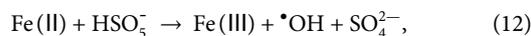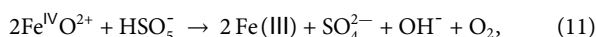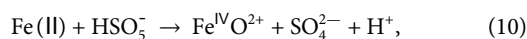
FIGURE 7
Identification of active species and possible degradation mechanism. **(A)** Impact of different quenchers on the TC degradation (Et-OH, TBA, L-His, and p-BQ) and **(B)** EPR spectra. Experiment conditions: 0.20 g/L catalyst, 10 mg/L TC, 1 mM PMS, initial pH = 3.01, and 30°C.

with 5,5-dimethylpyrroline (DMPO) and 2,2,6,6-tetramethyl-4-piperidinol (TEMP) as a spin trappers. In Figure 7B, the representative signals of 1:2:2:1 were observed, which represented DMPO-OH adducts. The formation of DMPO-•OH adducts may also result from the formation of Fe(IV) to transform DMPO. Since the DMPO-$SO_4^{\bullet-}$ adduct can translate to DMPO-OH adduct, the DMPO-$SO_4^{\bullet}$- adduct signal was not detected (Timmins Graham S et al., 1999). In addition, no TEMP-$^1O_2$ and DMPO-$O_2^{\bullet-}$ adducts were detected in the Fe-GMC systems, which was consistent with the results of the L-His and p-BQ quenching tests (Figure 7A). These results might be caused by the involvement of Fe(IV) in the Fe-GMC/PMS system (Equations 9–14) (Xiaowan et al., 2020; Shao et al., 2022).

$$Fe_3O_4 + 8H^+ \rightarrow Fe(II) + 2Fe(III) + 4H_2O, \tag{9}$$

$$Fe(II) + HSO_5^- \rightarrow Fe^{IV}O^{2+} + SO_4^{2-} + H^+, \tag{10}$$

$$2Fe^{IV}O^{2+} + HSO_5^- \rightarrow 2Fe(III) + SO_4^{2-} + OH^- + O_2, \tag{11}$$

$$Fe(II) + HSO_5^- \rightarrow Fe(III) + {}^{\bullet}OH + SO_4^{2-}, \tag{12}$$

$$Fe(II) + SO_4^{\bullet-} \rightarrow Fe(III) + SO_4^{2-}, \tag{13}$$

$$Fe(III) + HSO_5^- \rightarrow Fe(II) + SO_5^{\bullet-} + H^+. \tag{14}$$

Furthermore, we postulated the reaction mechanism underlying the removal of TC by •OH radicals. It is established that the TCs are susceptible to attack by reactive radicals such as •OH, $O_2^{\bullet-}$, and $^1O_2$ because they have three high-electron-density functional groups, namely, double bonds, phenolic groups, and amino groups. Supplementary Table S4 (Zhang et al., 2023) After the attack of •OH radical, TC will undergo demethylation and dehydration to produce intermediates 1 and 5 (Supplementary Figure S7), while intermediate 1 in the left pathway will continue to dehydration to produce 2, and the central carbon chain of intermediate 2 will break to produce intermediates 3 and 4, which will ultimately be degraded to CO_2 and H_2O.

Meanwhile, in the right pathway, •OH will attack the para or ortho position of the phenol ring of 2, and demethylation occurs to yield intermediate 6, which will undergo the reaction of ring-opening and de-hydroxylation to obtain intermediate 7, which ultimately produces CO_2 and H_2O.

To confirm the charge transfer between the catalysts, we conducted electrochemical tests on both GMC and Fe-GMC materials, as illustrated in Supplementary Figure S8. Upon the addition of PMS at 100 s, a notable alteration in current was observed for both GMC and Fe-GMC, indicative of electron transfer between the catalyst and PMS. Concurrently, the addition of TC to the system at 200 s resulted in a notable decline in the current of the Fe-GMC material compared to the GMC material. This observation suggests that the Fe-GMC/PMS system facilitated the acceleration of electron transfer.

4 Conclusion

In summary, the biochar carrier Fe-GMC synthesized can efficiently degrade TC in water under PMS catalysis. This study utilized goat manure and $FeSO_4 \cdot 7H_2O$ as sustainable feedstocks for composite catalysts and revealed the mechanism of TC degradation. The characterization results indicate that the Fe-GMC surface exhibits a porous structure, and the BET characterization results demonstrate that Fe-GMC possesses a substantial specific surface area of 416 m²/g. The TEM, XPS, and XRD results demonstrate that Fe was successfully loaded and existed as Fe₃O₄. In the Fe-GMC/PMS system, the primary degradation reaction is the •OH radical pathway, with charge transfer facilitated between Fe-GMC/PMS and TC. Moreover, the conditional experiments demonstrate that Fe-GMC exhibits excellent practical applicability and recycling potential. This work realizes the resource utilization of sheep manure waste and provides a new idea for removing antibiotics in the water environment, with excellent application prospects.

Data availability statement

The datasets presented in this study can be found in online repositories. The names of the repository/repositories and accession number(s) can be found in the article/Supplementary Material.

Author contributions

LF: writing–original draft, writing–review and editing, and data curation. QX: conceptualization and writing–original draft. YL: data curation and writing–review and editing. SZ: formal analysis and writing–review and editing. HL: investigation and writing–review and editing. SL: data curation and writing–review and editing. XL: conceptualization, writing–original draft, and writing–review and editing.

Funding

Conflict of interest

The authors declare that the research was conducted in the absence of any commercial or financial relationships that could be construed as a potential conflict of interest.

Publisher's note

All claims expressed in this article are solely those of the authors and do not necessarily represent those of their affiliated organizations, or those of the publisher, the editors and the reviewers. Any product that may be evaluated in this article, or claim that may be made by its manufacturer, is not guaranteed or endorsed by the publisher.

Supplementary material

The Supplementary Material for this article can be found online at: https://www.frontiersin.org/articles/10.3389/fenvs.2024.1467797/full#supplementary-material

References

Ahmadi, M., and Farshid, G. (2019). Organic dye degradation through peroxymonosulfate catalyzed by reusable graphite felt/ferriferrous oxide: mechanism and identification of intermediates. *Mater. Res. Bull.* 111, 43–52. doi:10.1016/j.materresbull.2018.10.027

Alireza, K., Fatemeh, S., Mehrangiz, F., Behnam, S., and Behrouz, V. (2015). Iron rich laterite soil with mesoporous structure for heterogeneous Fenton-like degradation of an azo dye under visible light. *J. Industrial Eng. Chem.* 26, 129–135. doi:10.1016/j.jiec.2014.11.024

Bolan, N., Hoang, S. A., Beiyuan, J., Gupta, S., Hou, D., Karakoti, A., et al. (2022). Multifunctional applications of biochar beyond carbon storage. *Int. Mater. Rev.* 67, 150–200. doi:10.1080/09506608.2021.1922047

Chang-Mao, H., Chiu-Wen, C., Yu-Zhe, J., and Cheng-Di, D. (2016). Fe₃O₄ magnetic nanoparticles: characterization and performance exemplified by the degradation of methylene blue in the presence of persulfate. *J. Adv. Oxid. Technol.* 19, 43–51. doi:10.1515/jaots-2016-0105

Chen, W., He, H., Lei, L., Zhu, K., He, D., Jin, H., et al. (2022). Green synthesis of novel Fe nanoparticles embedded in N-doped biochar composites derived from bagasse for sulfadiazine degradation via peroxymonosulfate activator: mechanism insight and performance assessment. *J. Water Process Eng.* 49, 103131. doi:10.1016/j.jwpe.2022.103131

Chen, X., Wang, X., and Fang, D. (2020). A review on C1s XPS-spectra for some kinds of carbon materials. *Fullerenes, Nanotub. Carbon Nanostructures* 28, 1048–1058. doi:10.1080/1536383x.2020.1794851

Da, O., Chen, Y., Jingchun, Y., Linbo, Q., Lu, H., and Chen, M. (2019). Activation mechanism of peroxymonosulfate by biochar for catalytic degradation of 1, 4-dioxane: important role of biochar defect structures. *Chem. Eng. J.* 370, 614–624. doi:10.1016/j.cej.2019.03.235

Dong, C., Chen, C., and Hung, C. (2017). Synthesis of magnetic biochar from bamboo biomass to activate persulfate for the removal of polycyclic aromatic hydrocarbons in marine sediments. *Bioresour. Technol.* 245, 188–195. doi:10.1016/j.biortech.2017.08.204

Fang, J., He, F., Yan, Z., Wang, J., Yu, R., and Zhou, H. (2024). Pyrite/biochar-activated peroxymonosulfate strengthens tetracycline degradation: important roles of surface functional groups and Fe(Ⅱ)/Fe(Ⅲ) redox cycling. *J. Environ. Chem. Eng.* 12 (3), 112923. doi:10.1016/j.jece.2024.112923

Guangfei, Y., Yuxian, W., Cao, H., He, Z., and Yongbing, X. (2020). Reactive oxygen species and catalytic active sites in heterogeneous catalytic ozonation for water purification. *Environ. Sci. Technol.* 54, 5931–5946. doi:10.1021/acs.est.0c00575

Guo, Y., Yan, L., Li, X., Yan, T., Song, W., Hou, T., et al. (2021). Goethite/biochar-activated peroxymonosulfate enhances tetracycline degradation: inherent roles of radical and non-radical processes. *Sci. Total Environ.* 783, 147102. doi:10.1016/j.scitotenv.2021.147102

Haitao, L., Qiang, G., Wang, G., Han, B., Xia, K., and Chenggang, Z. (2020). Architecturing CoTiO₃ overlayer on nanosheets-assembled hierarchical TiO₂ nanospheres as a highly active and robust catalyst for peroxymonosulfate activation and metronidazole degradation. *Chem. Eng. J.* 392, 123819. doi:10.1016/j.cej.2019.123819

Hussain, I., Mingyu, L., Yongqing, Z., Yichun, L., Shaobin, H., Du, X., et al. (2017). Insights into the mechanism of persulfate activation with nZVI/BC nanocomposite for the degradation of nonylphenol. *Chem. Eng. J.* 311, 163–172. doi:10.1016/j.cej.2016.11.085

Ikramullah, Z., and Zulkarnain, J. (2019). Identification of magnetite material (Fe₃O₄) based on natural materials as catalyst for industrial raw material application. *J. Phys. Conf. Ser.* 1232, 012054. doi:10.1088/1742-6596/1232/1/012054

Jayaselvan, L., Thanka, R. S., and Gnana, S. C. (2020). Structural and phase analysis of pure and metal ion doped Mn₂O₃ nanoparticles prepared by microwave assisted sol-gel method. *Rasayan J. Chem.* 13, 2223–2229. doi:10.31788/rjc.2020.1346083

Jiang, L. B., Yuan, X. Z., Zeng, G. M., Wu, Z. B., Liang, J., Chen, X. H., et al. (2018). Metal-free efficient photocatalyst for stable visible-light photocatalytic degradation of refractory pollutant. *Appl. Catal. B-Environmental* 221, 715–725. doi:10.1016/j.apcatb.2017.09.059

Jianghui, L., Lam, So H., and Wei, C. (2022). Degradation of 1-naphthylamine by a UV enhanced Fe²⁺/peroxymonosulfate system: a novel pH-dependent activation pathway. *Chem. Eng. J.* 443, 136299. doi:10.1016/j.cej.2022.136299

Li, Z., Wu, C., Yang, J., Guo, J., and Xiong, W. (2024). Efficiency and mechanism of phosphoric acid modified biochar loaded nanoscale zero-valent iron activated peroxymonosulfate for the degradation of bisphenol A. *Chem. Eng. Sci.* 295, 120132. doi:10.1016/j.ces.2024.120132

Luo, J., Shufeng, B., Yanan, Q., Qingda, A., Zuoyi, X., and Shangru, Z. (2020). Transforming goat manure into surface-loaded cobalt/biochar as PMS activator for highly efficient ciprofloxacin degradation. *Chem. Eng. J.* 395, 125063. doi:10.1016/j.cej.2020.125063

Luo, X., Shen, M., Liu, J., Ma, Y., Gong, B., Liu, H., et al. (2021). Resource utilization of piggery sludge to prepare recyclable magnetic biochar for highly efficient degradation of tetracycline through peroxymonosulfate activation. *J. Clean. Prod.* 294, 126372. doi:10.1016/j.jclepro.2021.126372

Luo, X., Zhang, L., Gong, X., Liu, Y., and Tian, J. (2023). Defect-enriched ilmenite-type catalyst derived from titanium dioxide slag for peroxymonosulfate activation in efficient tetracycline removal. *Chem. Eng. Sci.* 280, 119068. doi:10.1016/j.ces.2023.119068

Ma, Y., Xiong, D., Lv, X., Xuesong, Z., Chenchen, M., Xie, H., et al. (2021). Rapid and long-lasting acceleration of zero-valent iron nanoparticles@ Ti_3C_2-based MXene/peroxymonosulfate oxidation with bi-active centers toward ranitidine removal. *J. Mater. Chem. A* 9, 19817–19833. doi:10.1039/d1ta02046c

Masoumeh, G., Babak, K., Ahmadi, M., and Minoo, A. (2018). Photocatalytic activation of peroxymonosulfate by TiO_2 anchored on cupper ferrite (TiO2@ $CuFe_2O_4$) into 2, 4-D degradation: process feasibility, mechanism and pathway. *J. Hazard. Mater.* 359, 325–337. doi:10.1016/j.jhazmat.2018.06.069

Miguel, E., Andrés, H., and Francisco, M. (2022). Greenhouse gas emissions and carbon sequestration in organic dehesa livestock farms. Does technical-economic management matters? *J. Clean. Prod.* 372, 133779. doi:10.1016/j.jclepro.2022.133779

Mingfei, C., Yanhui, L., Yong, S., Huimin, W., Meixiu, L., Liubo, L., et al. (2021). Degradation of tetracycline in polluted wastewater by persulfate over copper alginate/graphene oxide composites. *J. Polym. Environ.* 29, 2227–2235. doi:10.1007/s10924-020-02038-6

Mohammadi, Z. A., and Saied Saeed Hosseiny, D. (2020). Ultra-high energy density supercapacitors based on metal–organic framework derived yolk–shell Cu–Co–P hollow nanospheres and $CuFeS_2$ nanosheet arrays. *Dalton Trans.* 49, 3353–3364. doi:10.1039/c9dt04897a

Nguyen, V., Nguyen, T. B., Chen, C., Hung, C., Huang, C. P., and Dong, C. (2019). Cobalt-impregnated biochar (Co-SCG) for heterogeneous activation of peroxymonosulfate for removal of tetracycline in water. *Bioresour. Technol.* 292, 121954. doi:10.1016/j.biortech.2019.121954

Pu, M., Jinquan, W., Zhang, F., Mark L, B., Ye, D., and Junfeng, N. (2021). Insight into degradation mechanism of sulfamethoxazole by metal-organic framework derived novel magnetic Fe@ C composite activated persulfate. *J. Hazard. Mater.* 414, 125598. doi:10.1016/j.jhazmat.2021.125598

Rahmat, Z. G., and Ahmadi, M. (2019). Activation of persulfate by Fe^{2+} for saline recalcitrant petrochemical wastewater treatment: intermediates identification and kinetic study. *Desalination Water Treat.* 166, 35–43. doi:10.5004/dwt.2019.24594

Ruan, X., Sun, Y., Du, W., Tang, Y., Qiang, L., Zhanying, Z., et al. (2019). Formation, characteristics, and applications of environmentally persistent free radicals in biochars: a review. *Bioresour. Technol.* 281, 457–468. doi:10.1016/j.biortech.2019.02.105

Shao, S., Xiaoshuai, L., Zhimin, G., Fan, B., Hu, J., Peng, J., et al. (2022). A new insight into the mechanism in Fe_3O_4@ CuO/PMS system with low oxidant dosage. *Chem. Eng. J.* 438, 135474. doi:10.1016/j.cej.2022.135474

Shuzhao, H., Di, Z., Fayaz, H., Liu, W., Su, J., Wang, D., et al. (2020). Structure, spectral analysis and microwave dielectric properties of novel x(NaBi) 0.5 MoO_4-(1-x) $Bi_2/3MoO_4$ (x= 0.2~ 0.8) ceramics with low sintering temperatures. *J. Eur. Ceram. Soc.* 40, 3569–3576. doi:10.1016/j.jeurceramsoc.2020.03.074

Song, T., Gao, Y., Ye, J., Zhang, X., Su, R., and Luo, J. (2022). Insight into enhanced degradation of tetracycline over peroxymonosulfate activated via biochar-based nanocomposite: performance and mechanism. *Environ. Sci. Pollut. Res.* 30 (10), 27394–27408. doi:10.1007/s11356-022-24102-5

Song, X., Zhang, Y., Luo, X., Chen, P., and Liu, J. (2019). 2D magnetic scallion sheathing-based biochar composites design and application for effective removal of arsenite in aqueous solutions. *Chem. Eng. Res. Des.* 152, 384–392. doi:10.1016/j.cherd.2019.10.007

Tang, H., Zhang, S., Pang, H., Wang, J., Xiangxue, W., Gang, S., et al. (2021). Insights into enhanced removal of U (VI) by melamine sponge supported sulfurized nanoscale zero-valent iron. *J. Clean. Prod.* 329, 129662. doi:10.1016/j.jclepro.2021.129662

Tianyi, D., Zhandong, L., Junjie, Z., Alex, E., and Dmitry, K. (2020). Nanoscale structural characterization of individual viral particles using atomic force microscopy infrared spectroscopy (AFM-IR) and tip-enhanced Raman spectroscopy (TERS). *Anal. Chem.* 92, 11297–11304. doi:10.1021/acs.analchem.0c01971

Timmins Graham, S., Liu, Ke J., Bechara Etelvino, J. H., Yashige, K., and Swartz Harold, M. (1999). Trapping of free radicals with direct *in vivo* EPR detection: a comparison of 5, 5-dimethyl-1-pyrroline-N-oxide and 5-diethoxyphosphoryl-5-methyl-1-pyrroline-N-oxide as spin traps for •HO and $SO_4^{•−}$. *Free Radic. Biol. Med.* 27, 329–333. doi:10.1016/s0891-5849(99)00049-0

Uthirakrishnan, U., Lu, X., Wang, J., Zhang, Z., Dai, J., Yujie, T., et al. (2020). Sulfate radicals-based advanced oxidation technology in various environmental remediation: a state-of-the-art review. *Chem. Eng. J.* 402, 126232. doi:10.1016/j.cej.2020.126232

Wang, H., Wang, H., Zhao, H., and Yan, Q. (2020). Adsorption and Fenton-like removal of chelated nickel from Zn-Ni alloy electroplating wastewater using activated biochar composite derived from Taihu blue algae. *Chem. Eng. J.* 379, 122372. doi:10.1016/j.cej.2019.122372

Wang, J., and Wang, S. (2018). Activation of persulfate (PS) and peroxymonosulfate (PMS) and application for the degradation of emerging contaminants. *Chem. Eng. J.* 334, 1502–1517. doi:10.1016/j.cej.2017.11.059

Wang, J., Zhi, D., Zhou, H., He, X., and Zhang, D. (2018). Evaluating tetracycline degradation pathway and intermediate toxicity during the electrochemical oxidation over a Ti/Ti_4O_7 anode. *Water Res.* 137, 324–334. doi:10.1016/j.watres.2018.03.030

Wang, Q., Lu, X., Ye, C., Jun, M., Jin, J., Bai, X., et al. (2017). Degradation of Bisphenol S by heat activated persulfate: kinetics study, transformation pathways and influences of co-existing chemicals. *Chem. Eng. J.* 328, 236–245. doi:10.1016/j.cej.2017.07.041

Wang, R., Wang, Q., Dong, L., and Zhang, J. (2021). Cleaner agricultural production in drinking-water source areas for the control of non-point source pollution in China. *J. Environ. Manag.* 285, 112096. doi:10.1016/j.jenvman.2021.112096

Wang, Z., Qiu, W., Pang, S., Qin, G., Chaoting, G., and Jin, J. (2022). Aqueous iron (IV)–oxo complex: an emerging powerful reactive oxidant formed by iron (II)-based advanced oxidation processes for oxidative water treatment. *Environ. Sci. Technol.* 56, 1492–1509. doi:10.1021/acs.est.1c04530

Wanying, X., Yi, Y., Wang, Y., Liu, D., Shen, Q., and Fangjie, Z. (2023). Hazard reduction and persistence of risk of antibiotic resistance during thermophilic composting of animal waste. *J. Environ. Manag.* 330, 117249. doi:10.1016/j.jenvman.2023.117249

Watanabe, N., Bergamaschi Brian, A., Loftin Keith, A., Meyer Michael, T., and Thomas, H. (2010). Use and environmental occurrence of antibiotics in freestall dairy farms with manured forage fields. *Environ. Sci. and Technol.* 17, 6591–6600. doi:10.1021/es100834s

Wu, L., Jin, T., Li, D., Wang, L., and Sun, Y. (2023). Heterogeneous activation of permonosulfate by biochar supporting CuCoFe layered double hydroxide for rapid degradation of phenanthrene. *J. Environ. Chem. Eng.* 11 (5), 110718. doi:10.1016/j.jece.2023.110718

Xiao, C., Wen-Da, O., and Teik-Thye, L. (2018). Graphene-and CNTs-based carbocatalysts in persulfates activation: material design and catalytic mechanisms. *Chem. Eng. J.* 354, 941–976. doi:10.1016/j.cej.2018.08.049

Xiaodong, L., Shen, J., Sun, Z., Liu, Y., Zhang, W., Wu, B., et al. (2021). Degradation of 2,4-dinitrotoluene using ferrous activated persulfate: kinetics, mechanisms, and effects of natural water matrices. *J. Environ. Chem. Eng.* 9, 106048. doi:10.1016/j.jece.2021.106048

Xiaohua, L., Liu, C., Chen, Y., Huang, H., and Ren, T. (2018). Antibiotic residues in liquid manure from swine feedlot and their effects on nearby groundwater in regions of North China. *Environ. Sci. Pollut. Res. Int.* 12, 11565–11575. doi:10.1007/s11356-018-1339-1

Xiaowan, L., Liu, X., Lin, C., Zhou, Z., He, M., and Ouyang, W. (2020). Catalytic oxidation of contaminants by Fe^0 activated peroxymonosulfate process: Fe (IV) involvement, degradation intermediates and toxicity evaluation. *Chem. Eng. J.* 382, 123013. doi:10.1016/j.cej.2019.123013

Xingyu, L., Borui, J., Lin, H., Zhongpei, D., Junyao, Q., Yiqiong, Y., et al. (2022). Application of sulfate radicals-based advanced oxidation technology in degradation of trace organic contaminants (TrOCs): recent advances and prospects. *J. Environ. Manag.* 308, 114664. doi:10.1016/j.jenvman.2022.114664

Yangju, L., Haoran, D., Long, L., Lin, T., Ran, T., Rui, L., et al. (2021). Recent advances in waste water treatment through transition metal sulfides-based advanced oxidation processes. *Water Res.* 192, 116850. doi:10.1016/j.watres.2021.116850

Zang, T., Wang, H., Liu, Y., Dai, L., Shuang, Z., and Shiyun, A. (2020). Fe-doped biochar derived from waste sludge for degradation of rhodamine B via enhancing activation of peroxymonosulfate. *Chemosphere* 261, 127616. doi:10.1016/j.chemosphere.2020.127616

Zhang, F., Huang, Z., Liu, Y.-Y., Zhang, Q., and Chang, C.-T. (2023). S–Modified MXene as a catalyst for accelerated tetracycline hydrochloride electrocatalytic degradation via ·OH and active chlorine triggering promotion. *Catalysts* 13 (9), 1237. doi:10.3390/catal13091237

Zhang, Y., Zhou, J., Chen, X., Wang, L., and Cai, W. (2019). Coupling of heterogeneous advanced oxidation processes and photocatalysis in efficient degradation of tetracycline hydrochloride by Fe-based MOFs: synergistic effect and degradation pathway. *Chem. Eng. J.* 369, 745–757. doi:10.1016/j.cej.2019.03.108

Zhijie, X., Yiping, F., Wang, F., Chen, D., Zhang, Q., Zeng, Y., et al. (2018). Construction of carbon dots modified $MoO_3/g-C_3N_4$ Z-scheme photocatalyst with enhanced visible-light photocatalytic activity for the degradation of tetracycline. *Appl. Catal. B-Environmental* 229, 96–104. doi:10.1016/j.apcatb.2018.02.011

Zhu, H., Guo, A., Siming, W., Yan, L., Guangyin, F., and Xiaojun, Y. (2022). Efficient tetracycline degradation via peroxymonosulfate activation by magnetic Co/N co-doped biochar: emphasizing the important role of biochar graphitization. *Chem. Eng. J.* 450, 138428. doi:10.1016/j.cej.2022.138428

Zhu, Y., Johnson, T. A., Su, J., Qiao, M., Guo, G., Stedtfeld, R. D., et al. (2013). Diverse and abundant antibiotic resistance genes in Chinese swine farms, *Proc. Natl. Acad. Sci. U. S. A., Diverse Abund. antibiotic Resist. Genes. Chin. swine farms.* 110, 3435–3440. doi:10.1073/pnas.1222743110

Zou, Y., Wentao, L., Lian, Y., Feng, X., Guangyu, A., Yue, W., et al. (2019). Activation of peroxymonosulfate by sp(2)-hybridized microalgae-derived carbon for ciprofloxacin degradation: importance of pyrolysis temperature. *Chem. Eng. J.* 370, 1286–1297. doi:10.1016/j.cej.2019.04.002